

ARTICLE

Self-doped conjugated polymers with electron-deficient quinone units for enhanced electron transport in highly efficient organic solar cells

Xi Luo | Jiangkai Yu | Haoran Tang  | Houji Cai | Wei Xiong | Kai Zhang | Fei Huang  | Yong Cao

Institute of Polymer Optoelectronic Materials and Devices, State Key Laboratory of Luminescent Materials and Devices, South China University of Technology (SCUT), Guangzhou, China

Correspondence

Haoran Tang and Fei Huang.
Email: mstanghaoran@scut.edu.cn and msfhuang@scut.edu.cn

Funding information

Basic and Applied Basic Research Foundation of Guangdong Province, Grant/Award Number: 2019B030302007; National Natural Science Foundation of China, Grant/Award Number: U21A6002; National Youth Foundation of China, Grant/Award Number: 52303227; State Key Laboratory of Luminescent Materials and Devices, Grant/Award Number: Skllmd-2023-12

Abstract

Organic solar cells (OSCs) have attracted significant attention as a burgeoning flexible technology, owing to their advanced power conversion efficiencies. Moreover, interface materials play a crucial role in optimizing energy level alignment between the active layer and electrodes, thereby enhancing carrier extraction within the device and improving efficiency. However, current methodologies for fabricating electron-transport materials with superior mobility are still limited compared with those for hole-transport materials. In this study, a benzodifurandione (BFDO)-derived building block with quinone resonance property and strong electron-withdrawing capability was synthesized. Two conjugated polymers, namely PBFDO-F6N and PBFDO-F6N-Br, were prepared, both of which exhibited good electron mobility and exceptional interface modification capabilities. A comprehensive investigation of the interaction between the interface layer and the active layer revealed that PBFDO-F6N induced doping at the acceptor interface. Additionally, the high mobility of PBFDO-F6N facilitated efficient carrier extraction at the interface. Consequently, the application of PBFDO-F6N as the cathode interface layer for PM6:BTP-eC9-based OSC devices resulted in a remarkable efficiency of 18.11%. Moreover, the device efficiency remained at ~96% even at a PBFDO-F6N interface thickness of 50 nm, demonstrating the great potential of this material for large-scale device preparation.

KEYWORDS

electron transport materials, organic solar cells, quinone structure, self n-doping

This is an open access article under the terms of the [Creative Commons Attribution](https://creativecommons.org/licenses/by/4.0/) License, which permits use, distribution and reproduction in any medium, provided the original work is properly cited.

© 2024 The Author(s). FlexMat published by John Wiley & Sons Australia, Ltd on behalf of Nanjing University of Posts & Telecommunications.

1 | INTRODUCTION

In recent years, organic solar cells (OSCs), an emerging flexible energy technology, have made rapid progress and have been successfully applied in wearable electronic systems, such as e-textiles and synthetic skins.^{1–10} The continuous research and development of active layer material systems has propelled the power conversion efficiency (PCE) of single-junction solar cells beyond the 19% threshold.^{11–20} Given the typical adoption of a multilayer device structure in OSCs, ensuring effective interfacial contact between distinct layers is crucial for achieving high-performance devices.^{21–25} Compared with hole transport, electron transport within organic material systems tends to exhibit lower efficiency and increased vulnerability to water and oxygen exposure.^{26,27} To ensure electron transport at the cathode, interfacial modification materials with a low work function (WF) are often employed to reduce the transport barrier.^{28–30} Water/alcohol-soluble conjugated polymers (WSCPs), composed of conjugated main chains and polar side chains, present a promising solution to interfacial problems. The water/alcohol solubility of WSCPs ensures their suitability for multilayer orthogonal solvent processing. Additionally, the conjugated backbone of these polymers facilitates electron transport, while the polar side chains enable dipole interaction with the electrodes, thereby modulating the WF.³¹ WSCPs, represented by poly[(9, 9-bis(3-(*N*, *N*-dimethylamino)propyl)-2, 7-fluorene)-*alt*-2, 7-(9, 9-dioctylfluorene)] (PFN), have been extensively utilized in various OSC applications.^{11,32–38} However, the conjugated chains of these polymers primarily consist of electron-donating units with limited electron mobility, resulting in device performance that is highly dependent on film thickness. This characteristic poses challenges for the fabrication of large-area devices. To address this issue, the incorporation of electron-deficient units into the conjugated backbone, which can enhance electron mobility, has been proposed. Currently, a variety of electron-deficient units have been adopted, such as diketopyrrolopyrrole (DPP),^{39–41} naphthalene diimide (NDI),^{42–44} and isoindigo (IID).⁴⁵ The thickness-insensitivity of the interface materials can be greatly improved. Additionally, one study reported that reducing the lowest unoccupied molecular orbital (LUMO) energy level facilitated the self-doping of side-chain polar groups onto the main chain, thereby leading to improved electron transport.⁴²

Furthermore, the presence of quinone resonance favors the π -conjugate extension of the molecular system with minimal distortion, thereby improving stacking and electron mobility.^{46–50} Studies have revealed that the quinone form of conjugated polymers exhibits higher

conductivity than the corresponding aromatic structure.^{51–53} The incorporation of blocks possessing quinone resonance into the conjugated backbone can also promote the doping characteristics of polymers.⁵⁴ However, most existing quinone-based building blocks exhibit limited electron-withdrawing capabilities, presenting challenges in achieving highly efficient electron transport at the cathode interface in OSCs.^{55,56} Therefore, the development of novel quinone-type building blocks with robust electron-deficient properties, along with the corresponding methods for constructing WSCPs, is significant for high-performance electron-transport interfacial materials.

Benzodifurandione (BFDO) has been recognized as a promising class of electron-deficient moieties utilized in the construction of polymers with advantageous electron transport properties in organic thermoelectric applications^{57–59} and organic transistors.^{60–62} BFDO demonstrates superior carrier delocalization compared with the commonly utilized NDI unit,⁶³ thereby facilitating the development of highly conductive *n*-type polymers.⁶⁴ However, current research primarily focuses on polymer synthesis via aldol condensation using the BFDO unit, thereby limiting the diversity of polymer species.^{65–68}

In this study, a BFDO-derived building block with quinone resonance properties and strong electron-withdrawing capability was developed. Two conjugated polymers, PBFDO-F6N and PBFDO-F6N-Br, were synthesized using Pd-catalyzed couplings. The introduction of the electron-deficient BFDO unit strongly reduced the LUMO level of the polymers, thereby enabling the realization of *n*-type transport properties. Moreover, the quinone structure introduced by the BFDO unit improved electron mobility. The measured conductivities of PBFDO-F6N and PBFDO-F6N-Br were 3.97×10^{-5} and 2.08×10^{-5} S cm⁻¹, respectively. These two polymers were employed as the electron transport layer (ETL) in OSC devices with a PM6:BTP-eC9 active layer. The highest efficiencies achieved with PBFDO-F6N and PBFDO-F6N-Br were 18.11% and 17.67%, respectively, representing some of the highest efficiencies obtained with the PM6:BTP-eC9 active layer. Furthermore, even at a thickness of 50 nm, the PCE of the devices with PBFDO-F6N as the ETL remained above 95%. This highlights the remarkable ability of the material to withstand thick film deposition, making it a promising candidate for the scalable production of OSC devices through roll-to-roll techniques. These results indicate that BFDO, an electron-deficient unit with quinone resonance properties, can effectively improve the electron transport of the polymer and is expected to achieve applications in other organic electronic devices.

2 | RESULTS AND DISCUSSION

We synthesized the bromine-substituted quinone derivatives of BFDO (BFDO-Br) using copper bromide and *N*-bromosuccinimide. The synthetic route and single crystal structure of BFDO-Br are depicted in Figure 1A,B and Figure S1, respectively. Detailed data for BFDO-Br single crystal are summarized in Table S1. After bromination, the C-C bond length of the furan ring was 1.347 Å, which is typically the length of alkene bonds.⁶⁹ Moreover, the bromine present on the prepared monomer exhibited Pd-catalyzed reactivity, enabling successful Stille coupling. This coupling expanded the conjugated backbone and promoted a benzo-quinone transition of the entire chain (Figure 1C). Both conjugated polymers, namely PBFDO-F6N and PBFDO-F6N-Br, were synthesized using this monomer. The polymers possessed both strong electron-withdrawing properties and quinone resonance properties compared with the previously reported electron-transport materials PFN and PNDIT-F3N (Figure 1D). This characteristic is instrumental for achieving polymers with enhanced electron mobility. The monomer characterizations involved are illustrated in Figure S2-S6. The number-average molecular weight (M_n) and molar mass dispersity ($\text{ĐM} = M_w/M_n$) of

PBFDO-F6N were 10.54 kDa and 1.338, respectively (Figure S7), as determined via gel permeation chromatography with chloroform as the mobile phase. The thermal behavior of PBFDO-F6N and PBFDO-F6N-Br was characterized through thermogravimetric analysis. The thermal decomposition temperature (5 wt% loss) of PBFDO-F6N was 273°C, while that of PBFDO-F6N-Br was slightly lower: 216°C (Figure S8). The great thermal stability of PBFDO-F6N and PBFDO-F6N-Br demonstrates their suitability for OSC applications.

We performed cyclic voltammetry measurements in acetonitrile to determine the LUMO levels and highest occupied molecular orbital (HOMO) levels of PBFDO-F6N and PBFDO-F6N-Br. The HOMO energy levels of PBFDO-F6N and PBFDO-F6N-Br were determined as -5.51 and -5.50 eV, respectively, according to the oxidation onset of the cyclic voltammetry curves (Figure S9). Similarly, the LUMO levels of PBFDO-F6N and PBFDO-F6N-Br were -4.01 and -4.30 eV, respectively, according to the reduction onset. The lower LUMO level of PBFDO-F6N-Br than that of PBFDO-F6N is attributable to the electrostatic and anion-induced polarization caused by anion- π interactions between the bromine anion and the electron-deficient unit.⁴² Notably, both polymers possessed LUMO energy levels below

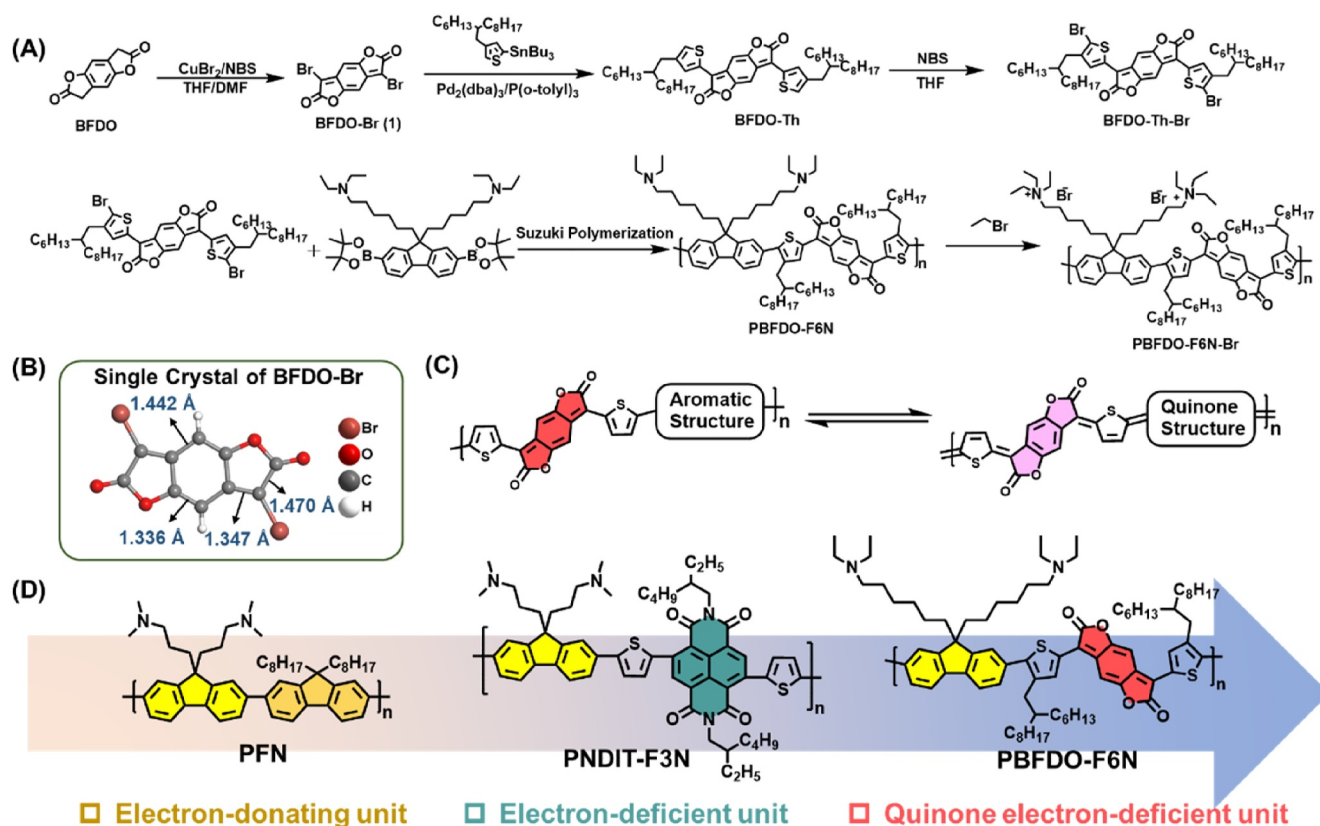


FIGURE 1 (A) Synthesis route of PBFDO-F6N and PBFDO-F6N-Br; (B) schematic of the BFDO-Br single crystal; (C) schematic of polymer quinone resonance facilitated by BFDO-Br; (D) comparison of PBFDO-F6N and previously reported PFN and PNDIT-F3N.

−4.0 eV, which is favorable for electron transfer from the non-fullerene acceptor to the cathode.

The ultraviolet-visible absorption spectra of the PBFDO-F6N and PBFDO-F6N-Br polymers (Figure 2A) exhibited similarity. The absorption peak at 350 nm corresponded to the absorbance associated with the π - π^* transition of the polymer backbone. Additionally, a subsequent absorption peak emerged at 700 nm, indicating intramolecular charge transfer (ICT) from the electron-rich fluorene units to the electron-deficient BFDO units.⁷⁰ PBFDO-F6N exhibited a more pronounced redshift in absorption than the previously reported PNDIT-F3N, indicating a stronger ICT within the material's main chain. This is attributable to the superior electron-absorbing capability of the BFDO unit to that of the NDI unit, which aligns with the deeper LUMO energy level observed in PBFDO-F6N.⁴² Furthermore, the reduction of the LUMO level can facilitate the transfer of lone-pair electrons from the side chain's amino group to the main chain, thereby realizing n-type self-doping.

To confirm this self-doping effect, both polymers were analyzed via X-ray photoelectron spectroscopy (XPS). The monomer exhibited two peaks, at 532.2 and 533.9 eV (Figure 2B), attributable to the oxygen of the carbonyl group and the furan ring, respectively. Both PBFDO-F6N and PBFDO-F6N-Br exhibited a new oxygen peak at

530.8 eV and a reduction in the intensity of the carbonyl O peak near 532 eV, indicating the presence of O^- within the polymers. This phenomenon is attributable to the self-doping process of the polymers.⁷¹ The nitrogen spectrum of PBFDO-F6N (Figure 2C) exhibited two distinct peaks: one peak around 399 eV and another near 402 eV, confirming the formation of positively charged N^+ . Therefore, electrons were transferred from N to the electron-deficient conjugated backbone, generating positively charged N^+ and negatively charged O^- . The PBFDO-F6N-Br spectrum exhibited only one peak, near 402 eV, indicating the completion of the quaternization reaction. The bromide ion, acting as a Lewis base, has been reported to achieve n-doping by undergoing ground-state charge transfer to the conjugated backbone,^{72,73} consistent with the O^- observed in PBFDO-F6N-Br. The newly generated O^- peak of PBFDO-F6N was higher than that of PBFDO-F6N-Br, indicating that the presence of the amino group resulted in a greater extent of n-doping in the conjugated backbone. This is beneficial for achieving higher electrical conductivity and electron transport capacity.

The self-doping process was further verified through electron spin resonance (ESR) characterization. The BFDO-Th produced a weak signal (Figure 2D), which substantiates the presence of a quinone structure in the

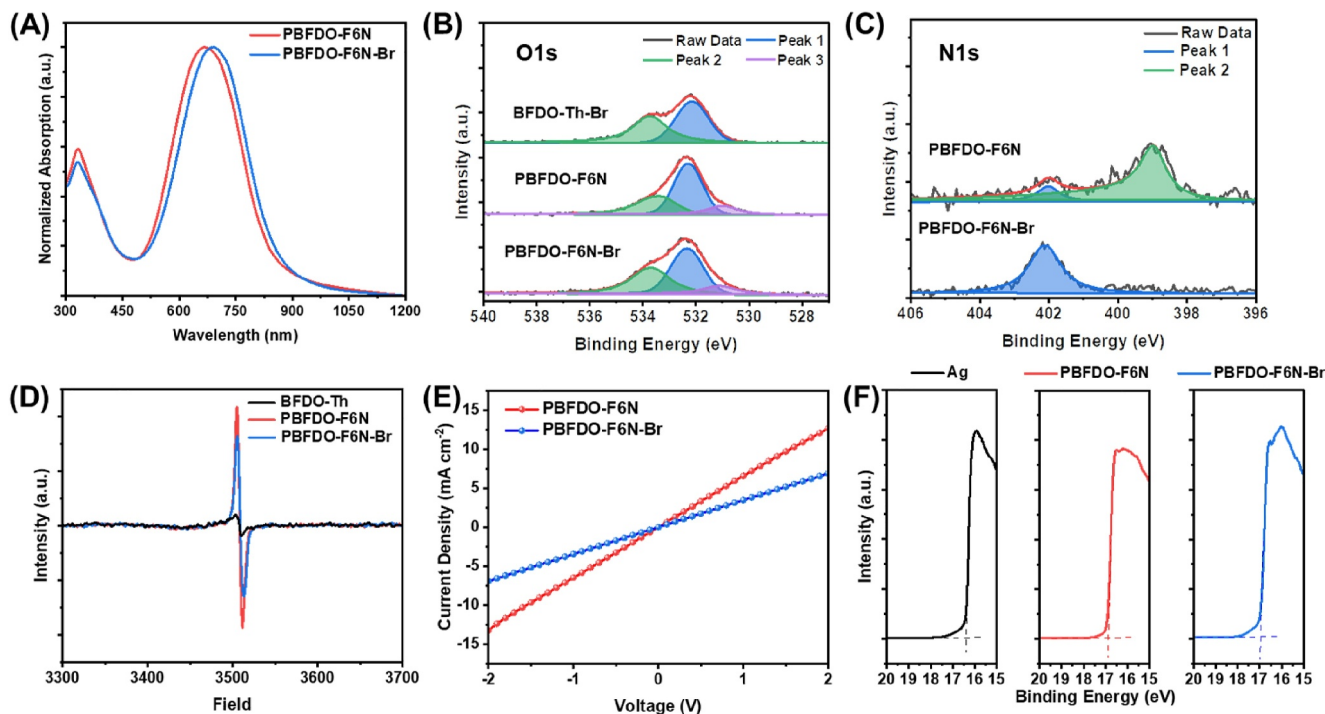


FIGURE 2 (A) UV-vis absorption spectra of PBFDO-F6N and PBFDO-F6N-Br in film; (B) O1s spectra of monomers BFDO-Th-Br, PBFDO-F6N, and PBFDO-F6N-Br; (C) N1s spectra of PBFDO-F6N and PBFDO-F6N-Br; (D) ESR spectra of BFDO-Th-Br, PBFDO-F6N, and PBFDO-F6N-Br in the solid state; (E) electrical conductivity measurements of PBFDO-F6N and PBFDO-F6N-Br; (F) UPS spectra of bare Ag, PBFDO-F6N, and PBFDO-F6N-Br. UPS, ultraviolet photoelectron spectroscopy; UV-vis, ultraviolet-visible.

monomer. The ESR signals of PBFDO-F6N and PBFDO-F6N-Br were quantified, and both materials exhibited robust ESR signals. Notably, the ESR signal intensity of PBFDO-F6N exceeded that of PBFDO-F6N-Br, suggesting that PBFDO-F6N possesses a higher degree of self-doping. This observation aligns with the XPS results. Subsequently, both polymers were subjected to conductivity measurements through the two-probe method.⁴⁰ A 60 nm-thick polymer film was sandwiched between the indium tin oxide (ITO) electrode and the Ag electrode. The current density (J)-voltage (V) relationship is illustrated in Figure 2E. PBFDO-F6N exhibited a higher conductivity ($3.97 \times 10^{-5} \text{ S cm}^{-1}$) than its quaternized polymer PBFDO-F6N-Br ($2.08 \times 10^{-5} \text{ S cm}^{-1}$), which is consistent with the higher doping level of the PBFDO-F6N.

Assessing electron-transport materials also involves suitable modifications to interface energy levels. The WF values of silver electrodes modified with the two conjugated polymers were determined via ultraviolet photoelectron spectroscopy. The WF values of PBFDO-F6N and PBFDO-F6N-Br were determined as 4.20 and 4.15 eV, respectively (Figure 2F). In comparison, the WF value of the unmodified Ag electrode was 4.72 eV. These findings indicate that two polymers could significantly reduce the WF values of the Ag electrodes through the interface dipole,⁷⁴ thereby facilitating efficient transfer and collection of electrons from the active layer to the cathode.⁷⁵

To explore the electron transport performances of the two polymers, they were applied as ETLs in OSC devices. The device structure adopted was ITO/PEDOT:PSS/PM6:BTP-eC9/ETL/Ag. For comparison, OSCs based on PNDIT-F3N- and PFN-series ETLs were also prepared. The device and chemical structures are illustrated in Figure 3A. The resulting J - V characteristics and external quantum efficiency (EQE) spectra are depicted in Figure 3B–C. The device with PBFDO-F6N as the ETL (5 nm) exhibited a maximum PCE of 18.11%, with an open-circuit voltage (V_{OC}) of 0.832 V, short-circuit current density (J_{SC}) of 27.83 mA cm^{-2} , and fill factor (FF) of 78.26%. The PCE was much higher than those of the control devices based on PNDIT-F3N (17.69%) and PFN (15.60%). The device based on PBFDO-F6N-Br exhibited a slightly lower performance, with a maximum PCE of 17.67%. Additionally, the PNDIT-F3N-based device exhibited a PCE of 17.69%, with a lower J_{SC} and FF than the PBFDO-F6N-based device. The J - V characteristics of the devices in the dark field are illustrated in Figure 3D. Notably, the devices based on PBFDO-F6N and PBFDO-F6N-Br exhibited low leakage currents, indicating a highly effective modification of the metal-semiconductor interface.

To investigate the underlying mechanism, we examined the interaction between the acceptor and the interface materials via ESR. The pure acceptor exhibited no ESR signal, whereas the mixed samples of BTP-eC9/PBFDO-F6N and BTP-eC9/PBFDO-F6N-Br exhibited

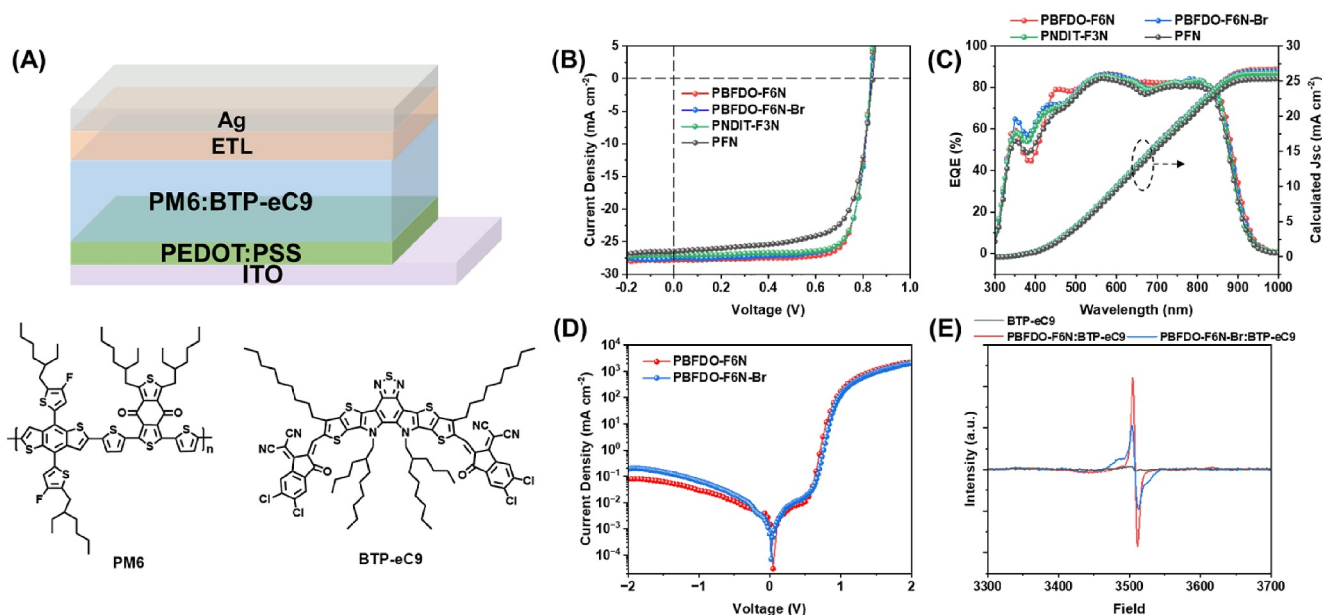


FIGURE 3 (A) Device structure and chemical structures of PM6 and BTP-eC9; (B) J - V curves of devices with PBFDO-F6N, PBFDO-F6N-Br, PNDIT-F3N, and PFN; (C) EQE curves of devices with PBFDO-F6N, PBFDO-F6N-Br, PNDIT-F3N, and PFN; (D) dark current versus voltage curves; (E) ESR spectra of BTP-eC9, PBFDO-F6N:BTP-eC9, and PBFDO-F6N-Br:BTP-eC9 blends in the solid state. EQE, external quantum efficiency.

significant signals (Figure 3E). While the strong ESR signals of the interface material may impact the measurement, the notably stronger signal observed in BTP-eC9/PBFDO-F6N indicates doping of the acceptor by PBFDO-F6N. Studies have shown that the amino group of PFN can effectively dope the non-fullerene acceptor. However, the poor electron transport characteristics of PFN resulted in charge accumulation at the interface, thereby hindering electron collection and deteriorating device performance.⁷⁶ The introduction of the electron-deficient BFDO unit into the conjugated backbone resulted in a significant reduction in the LUMO level. This modification prevented charge accumulation at the interface, thereby effectively enhancing the device's efficiency.

The electron mobility of a bilayer structure composed of the two polymer materials and BTP-eC9 was determined. The electron mobility was quantified using a space-charge-limited current (SCLC) model. Both materials exhibited notable electron mobility (Figure 4A), with the bilayer PBFDO-F6N-based device exhibiting an electron mobility of $3.56 \times 10^{-3} \text{ cm}^2 \text{ V}^{-1} \text{ s}^{-1}$, which was slightly higher than that of the PBFDO-F6N-Br-based device ($3.35 \times 10^{-3} \text{ cm}^2 \text{ V}^{-1} \text{ s}^{-1}$). Nevertheless, both materials exhibited excellent electron mobility at different thicknesses (Table S2). Furthermore, we performed light intensity-dependent measurements (Figure 4B). The α -values of the PBFDO-F6N- and PBFDO-F6N-Br-based devices were determined as 0.997 and 0.996, respectively. These high α -values suggest that both materials effectively inhibited bimolecular recombination. Additionally, the relationship between light intensity and V_{OC} was examined. The slope of the PBFDO-F6N-based device was $1.10 \text{ kT}/q$, while that of the PBFDO-F6N-Br-based device was $1.12 \text{ kT}/q$. The magnitude of the slope of V_{OC} versus light intensity serves as an indicator of the Shockley–

Read–Hall (SRH) recombination in devices.^{77,78} This suggests that the PBFDO-F6N-based device exhibited weaker trap-assisted recombination, which was consistent with its higher PCEs. The surface morphologies of the two polymers deposited on the active layer were characterized via atomic force microscopy. The root-mean-square roughness values of the active layer PM6:BTP-eC9 and the deposited polymers PBFDO-F6N and PBFDO-F6N-Br were 1.29, 1.09, and 1.22 nm, respectively (Figure S10). No significant difference was observed between PBFDO-F6N and PBFDO-F6N-Br.

Furthermore, we evaluated the electron transport capabilities of different materials by preparing OSC devices with thick-film ETLs. The J - V curves of devices with ETLs of different thicknesses are shown in Figure 5A–C, and their corresponding EQEs are shown in Figure 5D–F. The device parameters are summarized in Table 1. With the increase in the ETL thickness to 20 nm, the efficiencies of the PFN-based devices significantly declined to 8.16%. Conversely, the PNDIT-F3N-based device exhibited remarkable PCE retention. The device achieved a PCE of 16.49% at a thickness of 50 nm. The device with PBFDO-F6N as the ETL exhibited a notable PCE of 17.36% even at a thickness of 50 nm, retaining 95.9% of the value achieved with a 5 nm ETL. To further investigate the reasons for the thickness insensitivity of the PBFDO-F6N-based OSC devices, the devices based on PBFDO-F6N, PNDIT-F3N, and PFN were subjected to photo-injected linearly pressurized carrier extraction (photo-CELIV) measurements. The carrier mobility of the device with thin-film PBFDO-F6N was $3.57 \times 10^{-4} \text{ cm}^2 \text{ V}^{-1} \text{ s}^{-1}$ (Figure 5G). In comparison, the mobilities of the thin-film PNDIT-F3N- and PFN-based devices were 3.25×10^{-4} and $2.81 \times 10^{-4} \text{ cm}^2 \text{ V}^{-1} \text{ s}^{-1}$, respectively. These results indicate that the PBFDO-F6N-based OSC devices exhibited faster carrier transport,

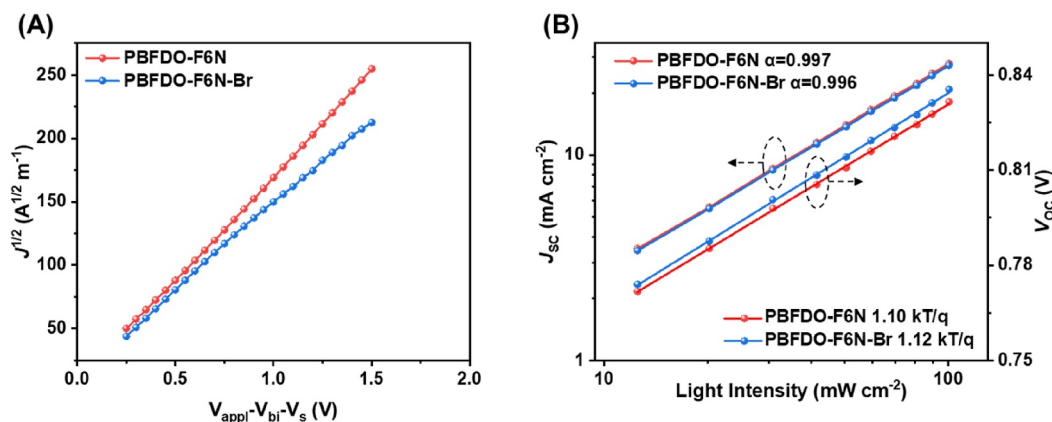


FIGURE 4 (A) SCLC measurement for bilayer electron-only devices; (B) light intensity dependence of J_{sc} and V_{oc} for OSCs devices with 5 nm ETL.

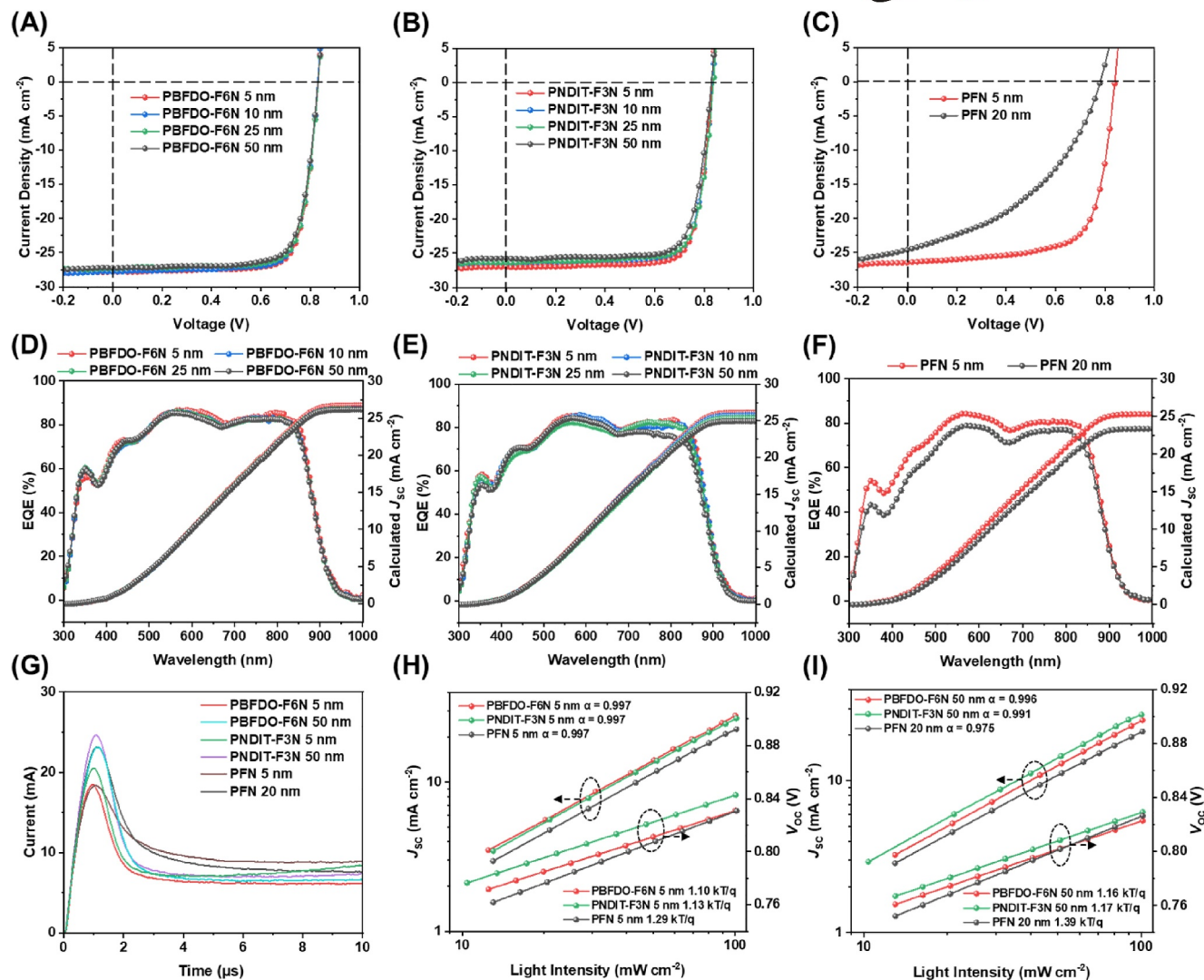


FIGURE 5 *J*-*V* curves of devices with (A) PBFDO-F6N, (B) PNDIT-F3N, and (C) PFN; corresponding EQE curves of (D) PBFDO-F6N, (E) PNDIT-F3N, and (F) PFN at various thicknesses; (G) photo-CELIV measurements of OSC devices with different ETLs; (H) light intensity dependence of *J*_{sc} and *V*_{oc} for devices with different 5-nm-thick ETLs; (I) light intensity dependence of *J*_{sc} and *V*_{oc} for devices with different ETLs at higher thicknesses. EQE, external quantum efficiency.

leading to reduced carrier recombination and enhanced *J*_{sc} and FF. Regarding the thick-film ETL-based devices, the carrier mobilities of PBFDO-F6N, PNDIT-F3N, and PFN were 2.87×10^{-4} , 2.85×10^{-4} , and $2.55 \times 10^{-4} \text{ cm}^2 \text{ V}^{-1} \text{ s}^{-1}$, respectively. The carrier mobility of the devices based on PBFDO-F6N and PNDIT-F3N remained significantly high, corresponding to the thickness-insensitive transport of both materials. Conversely, the PFN-based devices exhibited a substantial decrease in carrier mobility, resulting in carrier combination. Furthermore, light intensity-dependent measurements of the devices were conducted at different ETL thicknesses. Figure 5H-I display the light intensity dependence characterization results. The α value of the devices with PBFDO-F6N thick films was 0.996, indicating that the devices with thick-film ETLs

exhibited suppressed bimolecular recombination, demonstrating the superiority of PBFDO-F6N as an interface material. In contrast, the α value of PFN exhibited a more pronounced decline in thick-film devices. Additionally, the slopes of the *V*_{oc}-light intensity curves of devices with thin and thick PBFDO-F6N films were 1.10 and 1.16 kT/*q*, respectively. These values were lower than those of the devices based on PNDIT-F3N and PFN. This discrepancy suggests that SRH recombination was reduced in the PBFDO-F6N-based devices, which contributed to the higher PCE of the PBFDO-F6N-based OSC devices. Devices based on the quaternized products of the polymers were also fabricated. Compared with PNDIT-F3N-Br and PFN-Br, PBFDO-F6N-Br also exhibited greater film thickness insensitivity, with a higher PCE of up to 15.05% at a thickness of 50 nm

TABLE 1 Device performance of PM6:BTP-eC9-based OSCs with different ETLs at various thicknesses.

		Thickness (nm)	V_{OC} (V)	J_{SC} (mA/cm ²)	FF (%)	PCE (%)
PBFDO-F6N	Average	5	0.834 ± 0.003	27.73 ± 0.19	78.08 ± 0.35	18.05 ± 0.10
	Highest		0.832	27.83	78.26	18.11
	Average	10	0.830 ± 0.001	27.56 ± 0.31	77.56 ± 1.02	17.74 ± 0.12
	Highest		0.828	27.53	78.39	17.88
	Average	25	0.833 ± 0.001	27.29 ± 0.24	77.38 ± 1.37	17.57 ± 0.08
	Highest		0.832	27.34	77.78	17.70
	Average	50	0.833 ± 0.001	27.21 ± 0.18	75.47 ± 0.75	17.26 ± 0.09
	Highest		0.831	27.24	76.68	17.36
PNDIT-F3N	Average	5	0.833 ± 0.003	27.01 ± 0.30	77.75 ± 0.75	17.51 ± 0.19
	Highest		0.835	27.00	78.85	17.69
	Average	10	0.832 ± 0.002	26.53 ± 0.20	77.90 ± 0.44	17.19 ± 0.24
	Highest		0.834	26.69	78.40	17.45
	Average	25	0.833 ± 0.004	25.93 ± 0.30	77.51 ± 0.25	16.75 ± 0.29
	Highest		0.838	26.35	77.46	17.12
	Average	50	0.831 ± 0.003	25.67 ± 0.23	75.32 ± 3.64	16.06 ± 0.62
	Highest		0.830	25.75	77.18	16.49
PFN	Average	5	0.840 ± 0.001	26.33 ± 0.17	68.65 ± 1.53	15.19 ± 0.45
	Highest		0.840	26.49	70.07	15.60
	Average	20	0.620 ± 0.232	24.58 ± 0.40	34.77 ± 8.38	5.59 ± 3.00
	Highest		0.781	24.59	42.45	8.16

(Figure S11 and Table S3). In comparison, the PNDIT-F3N-Br- and PFN-Br-based devices exhibited PCEs of only 13.84% and 10.08% at 50 nm, respectively, which indicates that the introduction of quinone-type BFDO units effectively enhanced the electron transport capability of the conjugated materials.

To further elucidate the effect of different ETLs on the device performance, the electrochemical impedance test was performed. Figure S12 displays the impedance spectra of the devices based on PM6:BTP-eC9 with different ETLs and the equivalent circuit diagrams. Fitting the impedance spectra and equivalent circuits allowed for determining the series resistance (R_s), charge-transport resistance (R_{CT}), and geometrical capacitance (C) of corresponding devices. The obtained parameters were presented in Table S4. All devices exhibited similar R_s values. Notably, the devices utilizing PBFDO-F6N as ETLs exhibited lower R_{CT} values than those based on PFN, in both thin-film and thick-film conditions, suggesting superior charge transport capability for PBFDO-F6N.^{79–81}

The working mechanism is illustrated in Figure 6A,B. PBFDO-F6N exhibited a lower LUMO energy level and

enhanced electron mobility compared to PFN, thereby promoting electron transport at the interface, and satisfying the requirements of thick-film ETLs. To verify the versatility of the material, OSC devices with D18:L8-BO active layer and PBFDO-F6N as the ETL were also prepared (Figure S13). The J - V curves are shown in Figure 6C and Figure S14, and the detailed data are summarized in Table S5. The device with a 5 nm PBFDO-F6N as the ETL achieved a PCE of 18.69%. Remarkably, even with a thickness of 50 nm, the device maintained a PCE of 17.83%. This material, facilitating consistent performance across varying thicknesses, holds promise for the production of large-area flexible OSCs through the roll-to-roll technique.

3 | CONCLUSION

We synthesized a halogen-containing BFDO-based quinone resonance building block that retains strong electron-withdrawing capability and can be further expanded through Pd-catalyzed coupling reactions. This advancement significantly enhances the diversity of n-

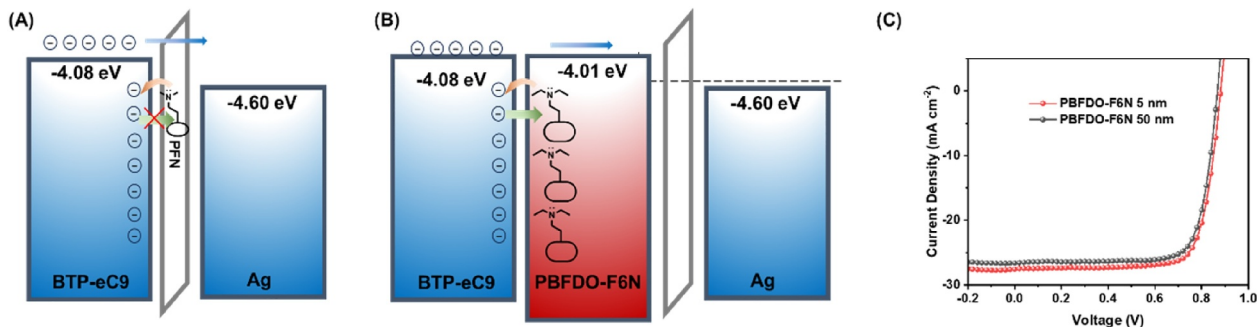


FIGURE 6 Charge transport modeling diagrams for cathode interface materials: (A) charge tunneling transport in PFN-based devices; (B) charge transport in PBFDO-F6N-based devices; (C) J - V curves of devices with PBFDO-F6N.

type conjugated polymers. Two conjugated polymers derived from this building block, namely PBFDO-F6N and PBFDO-F6N-Br, exhibited exceptional efficiency exceeding 18% when used as ETLs in OSCs. Moreover, the amino group in the side chain of PBFDO-F6N facilitated the n-doping of the non-fullerene acceptor while enabling self-n-doping. Along with the enhanced electron mobility facilitated by the quinone structure, PBFDO-F6N demonstrated remarkable efficiency retention of over 95%, even at a thickness of up to 50 nm, outperforming previously reported NDI-based thickness-insensitive ETL materials. Overall, this study provides alternative solutions for the advancement of large-scale flexible OSCs and contributes to the progress of electron-transport conjugated materials.

AUTHOR CONTRIBUTIONS

Xi Luo: Writing – original draft; Methodology; Validation; Visualization; Writing – review & editing; Investigation; Data curation; Conceptualization. **Jiangkai Yu:** Investigation; Validation; Formal analysis; Writing – original draft; Conceptualization; Methodology; Data curation; Visualization. **Haoran Tang:** Conceptualization; Funding acquisition; Writing – review & editing; Methodology; Validation; Project administration; Investigation. **Houji Cai:** Investigation; Methodology. **Wei Xiong:** Investigation. **Kai Zhang:** Investigation; Funding acquisition; Project administration; Validation; Supervision; Resources. **Fei Huang:** Funding acquisition; Methodology; Project administration; Formal analysis; Supervision; Resources; Writing – review & editing; Investigation; Conceptualization. **Yong Cao:** Supervision; Project administration; Resources; Funding acquisition.

ACKNOWLEDGMENTS

Xi Luo and Jiangkai Yu contributed equally to this work. This work was financially supported by the Basic and Applied Basic Research Major Program of Guangdong

Province (No. 2019B030302007), the National Natural Science Foundation of China (No. U21A6002), the National Youth Foundation of China (No. 52303227) and State Key Lab of Luminescent Materials and Devices, South China University of Technology (Skllmd-2023-12).

CONFLICT OF INTEREST STATEMENT

The authors declare no conflict of interests.

DATA AVAILABILITY STATEMENT

The data that support the findings of this study are available from the corresponding author upon reasonable request.

ORCID

Haoran Tang  <https://orcid.org/0000-0002-0963-7230>

Fei Huang  <https://orcid.org/0000-0001-9665-6642>

REFERENCES

1. Y. Sun, M. Chang, L. Meng, X. Wan, H. Gao, Y. Zhang, K. Zhao, Z. Sun, C. Li, S. Liu, H. Wang, J. Liang, Y. Chen, *Nat. Electron* **2019**, *2*, 513.
2. F. Qi, Y. Li, R. Zhang, F. R. Lin, K. Liu, Q. Fan, A. K. Y. Jen, *Angew. Chem. Int. Ed.* **2023**, *62*, e202303066.
3. Y. Hu, J. Wang, C. Yan, P. Cheng, *Nat. Rev. Mater.* **2022**, *7*, 836.
4. X. Zheng, L. Zuo, F. Zhao, Y. Li, T. Chen, S. Shan, K. Yan, Y. Pan, B. Xu, C.-Z. Li, M. Shi, J. Hou, H. Chen, *Adv. Mater.* **2022**, *34*, 2200044.
5. J. Wang, Y. Cui, Y. Xu, K. Xian, P. Bi, Z. Chen, K. Zhou, L. Ma, T. Zhang, Y. Yang, Y. Zu, H. Yao, X. Hao, L. Ye, J. Hou, *Adv. Mater.* **2022**, *34*, 2205009.
6. L. Xie, J. Zhang, W. Song, J. Ge, D. Li, R. Zhou, J. Zhang, X. Zhang, D. Yang, B. Tang, T. Wu, Z. Ge, *Nano Energy* **2022**, *99*, 107414.
7. X. Liu, Z. Zheng, J. Wang, Y. Wang, B. Xu, S. Zhang, J. Hou, X. Hou, *Adv. Mater.* **2022**, *34*, 2106453.
8. L. Ma, Y. Cui, J. Zhang, K. Xian, Z. Chen, K. Zhou, T. Zhang, W. Wang, H. Yao, S. Zhang, X. Hao, L. Ye, J. Hou, *Adv. Mater.* **2023**, *35*, 2208926.
9. X. Duan, W. Song, J. Qiao, X. Li, Y. Cai, H. Wu, J. Zhang, X. Hao, Z. Tang, Z. Ge, F. Huang, Y. Sun, *Energy Environ. Sci.* **2022**, *15*, 1563.

10. C. Xie, Y. Liu, W. Wei, Y. Zhou, *Adv. Funct. Mater.* **2023**, *33*, 2210675.
11. J. Fu, P. W. K. Fong, H. Liu, C.-S. Huang, X. Lu, S. Lu, M. Abdelsamie, T. Kodalle, C. M. Sutter-Fella, Y. Yang, G. Li, *Nat. Commun.* **2023**, *14*, 1760.
12. Y. Cui, Y. Xu, H. Yao, P. Bi, L. Hong, J. Zhang, Y. Zu, T. Zhang, J. Qin, J. Ren, Z. Chen, C. He, X. Hao, Z. Wei, J. Hou, *Adv. Mater.* **2021**, *33*, 2102420.
13. Y. Wei, Z. Chen, G. Lu, N. Yu, C. Li, J. Gao, X. Gu, X. Hao, G. Lu, Z. Tang, J. Zhang, Z. Wei, X. Zhang, H. Huang, *Adv. Mater.* **2022**, *34*, 2204718.
14. T. Chen, S. Li, Y. Li, Z. Chen, H. Wu, Y. Lin, Y. Gao, M. Wang, G. Ding, J. Min, Z. Ma, H. Zhu, L. Zuo, H. Chen, *Adv. Mater.* **2023**, *35*, 2300400.
15. J. Wang, Y. Wang, P. Bi, Z. Chen, J. Qiao, J. Li, W. Wang, Z. Zheng, S. Zhang, X. Hao, J. Hou, *Adv. Mater.* **2023**, *35*, 2301583.
16. L. Zhu, M. Zhang, J. Xu, C. Li, J. Yan, G. Zhou, W. Zhong, T. Hao, J. Song, X. Xue, Z. Zhou, R. Zeng, H. Zhu, C. C. Chen, R. C. I. MacKenzie, Y. Zou, J. Nelson, Y. Zhang, Y. Sun, F. Liu, *Nat. Mater.* **2022**, *21*, 656.
17. K. Jiang, J. Zhang, C. Zhong, F. R. Lin, F. Qi, Q. Li, Z. Peng, W. Kaminsky, S. H. Jang, J. Yu, X. Deng, H. Hu, D. Shen, F. Gao, H. Ade, M. Xiao, C. Zhang, A. K. Y. Jen, *Nat. Energy* **2022**, *7*, 1076.
18. K. Chong, X. Xu, H. Meng, J. Xue, L. Yu, W. Ma, Q. Peng, *Adv. Mater.* **2022**, *34*, 2109516.
19. G. Ding, T. Chen, M. Wang, X. Xia, C. He, X. Zheng, Y. Li, D. Zhou, X. Lu, L. Zuo, Z. Xu, H. Chen, *Nano-Micro Lett.* **2023**, *15*, 92.
20. B. Pang, C. Liao, X. Xu, L. Yu, R. Li, Q. Peng, *Adv. Mater.* **2023**, *35*, 2300631.
21. W. Lan, J. Gu, S. Wu, Y. Peng, M. Zhao, Y. Liao, T. Xu, B. Wei, L. Ding, F. Zhu, *EcoMat* **2021**, *3*, e12134.
22. Y. Lin, Y. Firdaus, F. H. Isikgor, M. I. Nugraha, E. Yengel, G. T. Harrison, R. Hallani, A. El-Labban, H. Faber, C. Ma, X. Zheng, A. Subbiah, C. T. Howells, O. M. Bakr, I. McCulloch, S. D. Wolf, L. Tsetseris, T. D. Anthopoulos, *ACS Energy Lett.* **2020**, *5*, 2935.
23. Y. Tao, D. Wang, X. He, H. Chen, C. Z. Li, *J. Mater. Chem. A* **2023**, *11*, 26277.
24. H. Tang, Y. Bai, H. Zhao, X. Qin, Z. Hu, C. Zhou, F. Huang, Y. Cao, *Adv. Mater.* **2024**, *36*, 2212236.
25. X. Y. Y. Cao, C. Liu, F. Huang, *Acta Polym. Sin.* **2022**, *53*, 307.
26. H. T. Nicolai, M. Kuik, G. A. H. Wetzelaer, B. de Boer, C. Campbell, C. Risko, J. L. Brédas, P. W. M. Blom, *Nat. Mater.* **2012**, *11*, 882.
27. Y. Zhang, B. de Boer, P. W. M. Blom, *Phys. Rev. B* **2010**, *81*, 085201.
28. C. He, Q. He, Y. He, Y. Li, F. Bai, C. Yang, Y. Ding, L. Wang, J. Ye, *Sol. Energy Mater. Sol. Cells* **2006**, *90*, 1815.
29. V. D. Mihailetchi, L. J. A. Koster, P. W. M. Blom, *Appl. Phys. Lett.* **2004**, *85*, 970.
30. M. O. Reese, M. S. White, G. Rumbles, D. S. Ginley, S. E. Shaheen, *Appl. Phys. Lett.* **2008**, *92*, 053307.
31. F. Huang, L. Hou, H. Wu, X. Wang, H. Shen, W. Cao, W. Yang, Y. Cao, *J. Am. Chem. Soc.* **2004**, *126*, 9845.
32. Y. Lin, Y. Zhang, A. Magomedov, E. Gkogkosi, J. Zhang, X. Zheng, A. El-Labban, S. Barlow, V. Getautis, E. Wang, L. Tsetseris, S. R. Marder, I. McCulloch, T. D. Anthopoulos, *Mater. Horiz.* **2023**, *10*, 1292.
33. L. Meng, Y. Zhang, X. Wan, C. Li, X. Zhang, Y. Wang, X. Ke, Z. Xiao, L. Ding, R. Xia, H.-L. Yip, Y. Cao, Y. Chen, *Science* **2018**, *361*, 1094.
34. T. R. Andersen, H. F. Dam, M. Hösel, M. Helgesen, J. E. Carlé, T. T. Larsen-Olsen, S. A. Gevorgyan, J. W. Andreasen, J. Adams, N. Li, F. Machui, G. D. Spyropoulos, T. Ameri, N. Lemaître, M. Legros, A. Scheel, D. Gaiser, K. Kreul, S. Berny, O. R. Lozman, S. Nordman, M. Välimäki, M. Vilkmann, R. R. Søndergaard, M. Jørgensen, C. J. Brabec, F. C. Krebs, *Energy Environ. Sci.* **2014**, *7*, 2925.
35. Z. Zheng, Q. Hu, S. Zhang, D. Zhang, J. Wang, S. Xie, R. Wang, Y. Qin, W. Li, L. Hong, N. Liang, F. Liu, Y. Zhang, Z. Wei, Z. Tang, T. P. Russell, J. Hou, H. Zhou, *Adv. Mater.* **2018**, *30*, 1801801.
36. J. Wang, Z. Zheng, Y. Zu, Y. Wang, X. Liu, S. Zhang, M. Zhang, J. Hou, *Adv. Mater.* **2021**, *33*, 2102787.
37. C. He, C. Zhong, H. Wu, R. Yang, W. Yang, F. Huang, G. C. Bazan, Y. Cao, *J. Mater. Chem.* **2010**, *20*, 2617.
38. Z. He, C. Zhang, X. Xu, L. Zhang, L. Huang, J. Chen, H. Wu, Y. Cao, *Adv. Mater.* **2011**, *23*, 3086.
39. L. Hu, F. Wu, C. Li, A. Hu, X. Hu, Y. Zhang, L. Chen, Y. Chen, *Macromolecules* **2015**, *48*, 5578.
40. X. Jin, Y. Wang, X. Cheng, H. Zhou, L. Hu, Y. Zhou, L. Chen, Y. Chen, *J. Mater. Chem. A* **2018**, *6*, 423.
41. Y. Tan, L. Chen, F. Wu, B. Huang, Z. Liao, Z. Yu, L. Hu, Y. Zhou, Y. Chen, *Macromolecules* **2018**, *51*, 8197.
42. Z. Wu, C. Sun, S. Dong, X.-F. Jiang, S. Wu, H. Wu, H. L. Yip, F. Huang, Y. Cao, *J. Am. Chem. Soc.* **2016**, *138*, 2004.
43. A. Sharma, S. Singh, X. Song, D. Rosas Villalva, J. Troughton, D. Corzo, L. Toppare, G. Gunbas, B. C. Schroeder, D. Baran, *Chem. Mater.* **2021**, *33*, 8602.
44. Y. Liu, Z. A. Page, T. P. Russell, T. Emrick, *Angew. Chem. Int. Ed.* **2015**, *54*, 11485.
45. L. Yang, S. Shen, X. Chen, H. Wei, D. Xia, C. Zhao, N. Zhang, Y. Hu, W. Li, H. Xin, J. Song, *Adv. Funct. Mater.* **2023**, *33*, 2303603.
46. Y. Qiao, Y. Guo, C. Yu, F. Zhang, W. Xu, Y. Liu, D. Zhu, *J. Am. Chem. Soc.* **2012**, *134*, 4084.
47. T. Du, Y. Liu, C. Wang, Y. Deng, Y. Geng, *Macromolecules* **2022**, *55*, 5975.
48. Y. Deng, B. Sun, Y. He, J. Quinn, C. Guo, Y. Li, *Angew. Chem. Int. Ed.* **2016**, *55*, 3459.
49. T. Du, R. Gao, Y. Deng, C. Wang, Q. Zhou, Y. Geng, *Angew. Chem. Int. Ed.* **2020**, *59*, 221.
50. J. Chen, W. Zhang, L. Wang, G. Yu, *Adv. Mater.* **2023**, *35*, 2210772.
51. J. L. Brédas, *J. Chem. Phys.* **1985**, *82*, 3808.
52. W. Rüttinger, G. C. Dismukes, *Chem. Rev.* **1997**, *97*, 1.
53. J. L. Brédas, B. Thémans, J. G. Fripiat, J. M. André, R. R. Chance, *Phys. Rev. B* **1984**, *29*, 6761.
54. H. Tang, Z. Liu, Y. Tang, Z. Du, Y. Liang, Z. Hu, K. Zhang, F. Huang, Y. Cao, *Giant* **2021**, *6*, 100053.
55. H. Hwang, Y. Kim, M. Kang, M.-H. Lee, Y. J. Heo, D.-Y. Kim, *Polym. Chem.* **2017**, *8*, 361.
56. H. Hwang, D. Khim, J.-M. Yun, E. Jung, S. Y. Jang, Y. H. Jang, Y. Y. Noh, D. Y. Kim, *Adv. Funct. Mater.* **2015**, *25*, 1146.
57. Y. Lu, Z. D. Yu, R. Z. Zhang, Z. F. Yao, H. Y. You, L. Jiang, H. I. Un, B.-W. Dong, M. Xiong, J. Y. Wang, J. Pei, *Angew. Chem. Int. Ed.* **2019**, *58*, 11390.

58. Z. D. Yu, Y. Lu, Z. Y. Wang, H.-I. Un, S. J. Zelewski, Y. Cui, H. Y. You, Y. Liu, K.-F. Xie, Z. F. Yao, Y. C. He, J. Y. Wang, W. B. Hu, H. Siringhaus, J. Pei, *Sci. Adv.* **2023**, 9, eadf3495.
59. C. Y. Yang, W. L. Jin, J. Wang, Y.-F. Ding, S. Nong, K. Shi, Y. Lu, Y. Z. Dai, F. D. Zhuang, T. Lei, C. A. Di, D. Zhu, J. Y. Wang, J. Pei, *Adv. Mater.* **2018**, 30, 1802850.
60. Y. Q. Zheng, T. Lei, J. H. Dou, X. Xia, J. Y. Wang, C. J. Liu, J. Pei, *Adv. Mater.* **2016**, 28, 7213.
61. Y. Z. Dai, N. Ai, Y. Lu, Y. Q. Zheng, J. H. Dou, K. Shi, T. Lei, J. Y. Wang, J. Pei, *Chem. Sci.* **2016**, 7, 5753.
62. Z. F. Yao, H. T. Wu, F. D. Zhuang, P. F. Zhang, Q. Y. Li, J. Y. Wang, J. Pei, *Small* **2024**, 20, 2306010.
63. Y. Lu, Z. D. Yu, H.-I. Un, Z.-F. Yao, H. Y. You, W. Jin, L. Li, Z. Y. Wang, B. W. Dong, S. Barlow, E. Longhi, C. A. Di, D. Zhu, J. Y. Wang, C. Silva, S. R. Marder, J. Pei, *Adv. Mater.* **2021**, 33, 2005946.
64. H. Tang, Y. Liang, C. Liu, Z. Hu, Y. Deng, H. Guo, Z. Yu, A. Song, H. Zhao, D. Zhao, Y. Zhang, X. Guo, J. Pei, Y. Ma, Y. Cao, F. Huang, *Nature* **2022**, 611, 271.
65. H. Tang, Y. Dou, R. Tan, Z. Chen, C. Liu, K. Zhang, J. Zhang, F. Huang, Y. Cao, *Polym. J.* **2023**, 55, 517.
66. H. Zhao, Y. Dou, S. Chen, H. Tang, Y. Bai, R. Tan, K. Zhang, C. Liu, F. Huang, *Chem. Mater.* **2023**, 35, 8695.
67. Z. F. Yao, H.-Y. Liu, Z. Y. Wang, Z.-K. Zhou, J. Y. Wang, J. Pei, *Chem-Asian J* **2019**, 14, 1686.
68. J. H. Dou, Y. Q. Zheng, Z.-F. Yao, T. Lei, X. Shen, X. Y. Luo, Z. A. Yu, S. D. Zhang, G. Han, Z. Wang, Y. Yi, J. Y. Wang, J. Pei, *Adv. Mater.* **2015**, 27, 8051.
69. M. B. Smith, *March's Advanced Organic Chemistry: Reactions, Mechanisms, and Structure*, John Wiley & Sons, **2020**.
70. Z. Chen, Z. Hu, Z. Wu, X. Liu, Y. Jin, M. Xiao, F. Huang, Y. Cao, *J. Mater. Chem. A* **2017**, 5, 19447.
71. K. Yang, X. Zhang, A. Harbuzaru, L. Wang, Y. Wang, C. Koh, H. Guo, Y. Shi, J. Chen, H. Sun, K. Feng, M. C. Ruiz Delgado, H. Y. Woo, R. P. Ortiz, X. Guo, *J. Am. Chem. Soc.* **2020**, 142, 4329.
72. D. X. Cao, D. Leifert, V. V. Brus, M. S. Wong, H. Phan, B. Yurash, N. Koch, G. C. Bazan, T. Q. Nguyen, *Mater. Chem. Front.* **2020**, 4, 3556.
73. J. W. Jo, J. W. Jung, S. Bae, M. J. Ko, H. Kim, W. H. Jo, A. K. Y. Jen, H. J. Son, *Adv. Mater. Interfaces* **2016**, 3, 1500703.
74. C. Feng, X. Wang, Z. He, Y. Cao, *Sol. RRL* **2021**, 5, 2000753.
75. G. Xu, L. Gao, H. Xu, L. Huang, Y. Xie, X. Cheng, Y. Li, L. Chen, Y. Chen, *J. Mater. Chem. A* **2017**, 5, 13807.
76. Q. Kang, Q. Wang, C. An, C. He, B. Xu, J. Hou, *J. Energy Chem.* **2020**, 43, 40.
77. A. K. K. Kyaw, D. H. Wang, V. Gupta, W. L. Leong, L. Ke, G. C. Bazan, A. J. Heeger, *ACS Nano* **2013**, 7, 4569.
78. Y. Qin, M. A. Uddin, Y. Chen, B. Jang, K. Zhao, Z. Zheng, R. Yu, T. J. Shin, H. Y. Woo, J. Hou, *Adv. Mater.* **2016**, 28, 9416.
79. A. Azeez, K. S. Narayan, *Appl. Phys. Lett.* **2020**, 117, 043302.
80. G. Garcia-Belmonte, A. Munar, E. M. Barea, J. Bisquert, I. Ugarte, R. Pacios, *Org. Electron.* **2008**, 9, 847.
81. H. Meng, C. Liao, M. Deng, X. Xu, L. Yu, Q. Peng, *Angew. Chem. Int. Ed.* **2021**, 60, 22554.

SUPPORTING INFORMATION

Additional supporting information can be found online in the Supporting Information section at the end of this article.

How to cite this article: X. Luo, J. Yu, H. Tang, H. Cai, W. Xiong, K. Zhang, F. Huang, Y. Cao, *FlexMat* **2024**, 1, 105. <https://doi.org/10.1002/flm2.17>